

Investigation of materials flow during the cold-rolling process by experimental evidence and numerical approaches

János György Bátorfi^{a,b*}, Gyula Pál^{a,b}, Purnima Chakravarty^{a,b}, Juriij Sidor^a

^a ELTE, Faculty of Informatics, Savaria Institute of Technology

^b ELTE, Faculty of Science, Doctoral School of Physics

ABSTRACT

In this paper, the modeling possibilities applicable to rolling processes were summarized, with particular reference to finite element models (FEM) and different flow-line models (FLM). The results of the analysis suggest that the different models are suitable for the study of deformation processes during cold rolling. Furthermore, the possibilities for the extension of the FLM model are summarized.

Keywords: *aluminum, cold rolling, FEM, flow-line model, material model, plastic deformation*

1. Introduction

Rolling means the plastic deformation of a sheet between rotating rolls, the thickness of the sheet is smaller after deformation than before it [1]. A simple geometrical drawing is shown in Fig. 1.

Because of the sheet's constant volume, the other two geometrical dimensions should be modified. Based on the results summarized in [2], the changes in the width can be neglected, so the relative change in the thickness dimension should be equal to the relative change in the sheet's length. For the notation of directions during the calculations, the following rules can be applied, which rules are the same as those applied in [3, 4]:

- x , RD , or 1 means the direction along the sheet's length,
- y , TD , or 2 means the direction along the sheet's width,
- z , ND , or 3 means the direction along the sheet's thickness.

The relation between the rolls' velocities can be different based on the type of the rolling process. In the case of symmetric rolling, the velocities are equal to each other, but in the case of asymmetric rolling, the velocities are different [1, 5]. This difference explains the difference in strain conditions: In the case of symmetric rolling, the characteristic types of strains are normal directional ones, but for asymmetric arrangement it is different, the shear types are typical on it [1, 3, 6, 7]. The effect of strain in different directions, i.e., normal and shear strains can be investigated by various measuring methods. The most well-documented and precious methods are the electron [1, 8–10] and X-ray [11–13] based methods, which are used for determining the relative amount of differently oriented grains. These techniques are developed by measuring the characteristic/typical texture components [1, 4, 8, 9, 14]. By knowing the amount of these texture components, it is possible determine the anisotropic and generally plastic-elastic properties of the deformed materials. The applicable options are for example the CP-FEM [15–21] or VPSC [22–26] models.

There are different methods for calculating the components and the equivalent value of the strain,

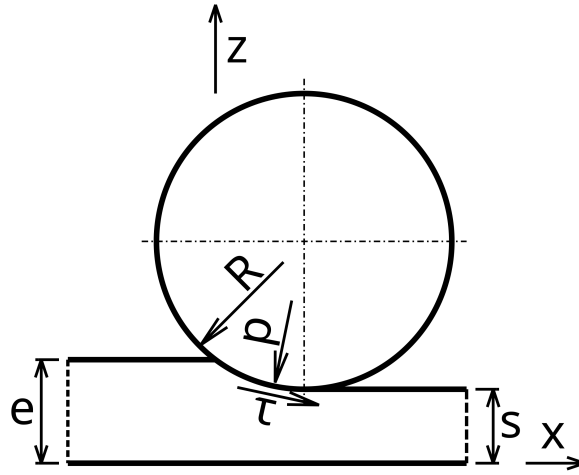


Figure 1. Applied geometry for simulations

in this study we have applied the version described in [14, 27–29]. The strain in the normal direction can be calculated by using Eq. (1) [27]:

$$\varepsilon_n = \frac{h_i - h_f}{h_i}, \tag{1}$$

where, ε_n is the strain in the normal direction, h_0 is the sheet’s thickness before rolling, and h_f is the sheet’s thickness after rolling.

The measurable shear can be calculated by using Eq. (2) [27]:

$$\gamma = \frac{dx}{dz}, \tag{2}$$

where γ is a derivative of displacement of the sheet in the rolling direction.

The calculated shear strain contains the effect of shear and the reduction of the sheet’s thickness [27]:

$$\varepsilon_S = \frac{2(1 - \varepsilon_n)^2}{\varepsilon_n(2 - \varepsilon_n)} \gamma \cdot \ln \frac{1}{1 - \varepsilon_n}, \tag{3}$$

where, ε_S is the calculated value of the shear strain.

The value of equivalent strain was calculated from the previously calculated shear strain [27]:

$$\varepsilon_{eq} = \sqrt{\frac{4}{3} \left(\ln \left(\frac{1}{1 - \varepsilon_n} \right) \right)^2 + \frac{\varepsilon_S^2}{3}}, \tag{4}$$

where, ε_{eq} is the equivalent strain.

The other important parameters, which can be used during the description of the deformation processes, are the “coefficient of friction (COF)”, and the “roll gap parameter”. The friction coefficient means the rate of the maximal slip stress and the normal pressure [30], there are many other, similar parameters for describing this phenomenon [31–33]. On other hand, there are more parameters that can be applied during this calculation [34, 35], but in our study, we have used only the geometrical parameters for calculating a minimal value of the coefficient of friction [36]. The theory under consideration is presented by Eq. (5).

$$\mu_{min} = \frac{1}{2} \sqrt{\frac{h}{R}} \frac{\ln\left(\frac{h_o}{h_f}\right) + \frac{1}{4} \sqrt{\frac{h_o - h_f}{R}}}{\tan^{-1}\left(\frac{h_o}{h_f} - 1\right)}, \quad (5)$$

where, μ_{min} is a calculated minimal value of the coefficient of friction.

However, in case of more precise calculations and simulations, it is necessary, to use a corrected value of coefficient of friction; this correction is achieved by applying Eq. (6). The correction factor expresses the effect of the neglected parameters for example roughness, the local change of the temperature, the contact pressure, and the slip velocity between the rolls and the sheet [30].

$$\mu_{mod} = C_f \cdot \mu_{min}, \quad (6)$$

where, μ_{mod} is the corrected value of the friction coefficient and C_f is the correction factor. The correction factor has a value of 1.1-1.4-1.5 [20, 21, 37]. Another approximation is using a constant 0.07-0.08 value, as it is described in [3].

The last, following examined important parameter is the effect of the roll gap, which documents not only the geometry of the sheet, but also the dimensions of the rolls is a significant factor [38]. This effect can be taken into account by using the parameter L/R based on simple geometrical calculations, which is described in Eq. (7).

$$\frac{L}{R} = \sqrt{\frac{h_i - h_f}{R}}, \quad (7)$$

where, L/R is the ‘‘roll gap parameter’’ and L is the length of the pressed surface.

During this study, we have examined the cold rolling of aluminum sheets, and the modeling options, mainly the finite element method and the flowline model.

2. Material model

The modeling of plastic deformation during specific manufacturing processes needs a mechanical material model for deformation. This model can be developed by different standard material examinations. The most commonly used methods applied for determining the deformation stress belongs to different value of strain, strain rate, and temperature. The examined material in this research is Aluminum (Al), which has various stress responses for different groups of material parameters. We examined the material about the room temperature (20-25 °C) [39, 40] and a relatively small strain rate. It has been summarized in different literature sources [41, 42], that for these parameter sets the effect of temperature and strain are subject of ignorance. These parameters are neglected because the room temperature (which has been the temperature of the specimen during the tensile test) is 40% below the melting point of Al-1050 material, which reduced the value of recrystallization temperature to 380-410 °C [43]. The Ramberg-Osgood material model [44, 45], which was used for the Finite Element Simulation (FEM), was chosen from the general material model programmed in the applied DEFORM 2D [46] FEM software by a slightly different form. The applied equation is shown in Eq. (8), and the material parameters of the equation are the following, based on the measured values of [37]: the elasticity modulus (E) is 69.9 GPa, the hardening coefficient (K) is 144.6 MPa and the hardening exponent is 0.370 and these parameters were determined from the tensile test.

$$\varepsilon = \frac{\sigma}{E} + \left(\frac{\sigma}{K}\right)^{1/c} \quad (8)$$

3. Modeling approaches

There are several approaches used for the simulation of the rolling. The three main groups can be defined by the modeling principles: simple geometrical, analytical and ones based on principles of continuum mechanics. However, the accuracy of the geometric model is relatively low due to the simplifications of complex processes. These models also use 2D [47] or 3D [48] approximations. On the other hand, it is possible to improvise these models by modifying a few parameters, that can be determined by various measurements or can be found in various literature sources. These methods for different types of rolling (hot/cold, symmetric/asymmetric) are described among others in [1, 14, 21, 49, 50].

The second group includes those methods, which are valid and applicable only to a small group of general manufacturing processes. They use fewer approximations, for example; using a simple material model by neglecting the effect of generated heat during the plastic deformation, and using a theoretical function for describing the relations between various parameters. These types of modelling techniques however have a giant advantage compared to the third group, they have a significantly higher simulation speed because they use explicit numerical methods, which provide the interpretation that the required temperature and mechanical parameters can be calculated for an arbitrary time and coordinates of the workpiece. The most commonly used examples for this group of modeling approaches are the “flowline models (FLM)”. There are several types of FLMs that can be used for calculating the deformation processes of forming manufacturing technologies beyond the rolling [51–54], for example, “(non)equal-channel angular pressing ((N)ECAP)” [55–57].

The third modeling group consists of the numerical methods. The typical example is the “finite element method (FEM)”, but there are many others, for example, the “upper bound method” [58, 59], the “uniform strain field method” [54, 60], or the “finite difference method” [54, 61]. The FEM is based on dividing the geometry into smaller parts, and the mechanical, thermodynamical, and crystallographic theories can be applied to these smaller parts for individual timesteps. The calculation is simpler for one element, but due to the large number of elements and timesteps, the calculation takes a long time. The advantage of the FEM method is, that the mechanical and thermodynamical material laws can be modified for individual materials. In addition, the contacts, properties, and the applied simplifications can be defined by user in the software. The models can be extended by crystallographic and texture calculations for determining the anisotropic and general mechanical properties of the deformed material. Examples for applying the FEM to modeling the rolling process can be found in literature [1, 3, 5, 49, 50, 52, 53, 62–68].

4. Flowline model

Different versions of the FLM models are based on simple continuity principles [51]. The models use an approximating function to describe streamlines/flowlines, described by Eq. (9) [51, 52], where the streamline means the material’s flow along a prescribed path, by examining the motion of rollgap’s points [52].

$$\Phi(x, z) = z \left[1 + \left(\alpha + \frac{(1 - \alpha)(x - d)^2}{d^2} \right)^{-n} \right]^{1/n} = \frac{z_s}{\alpha}, \quad (9)$$

where, Φ is the streamline function, x , z are coordinate values on the sheet as defined earlier in Fig. 1, z_s is the relative position of the rolled sheet’s thickness.

There are other important parameters, which are used by the FLM model. These parameters are described in Eq. (10)-(12) [51].

$$\alpha = \frac{s}{e}, \quad (10)$$

where, s is half-thickness after the rolling, and e is the half-thickness prior rolling.

$$\cos(\theta) = \frac{R + s - e}{R}, \quad (11)$$

where, θ is the press angle.

$$d = R \sin(\theta), \quad (12)$$

where, d is the projected length of the pressured surface.

The following important parameters are different components of the velocity field on the sheet's cross-section. These velocities can be calculated by Eq. (13) and (14).

$$v_x(x, z) = \lambda(x, z) \frac{\partial \Phi(x, z)}{\partial z}, \quad (13)$$

$$v_z(x, z) = -\lambda(x, z) \frac{\partial \Phi(x, z)}{\partial x}. \quad (14)$$

where, v_x and v_z are the velocities of a point in directions x and z .

The calculation of the velocity values needs to have the $\lambda(x, z)$ function in the form of Eq. (15), which can be determined from the velocity boundary conditions.

$$\lambda(x, z) = \frac{v_x(x = d, z)}{(\alpha^{-n} + 1)^{1/n}}. \quad (15)$$

where, $v_x(x = d, z)$ is the velocity at the exit point of the streamline, it can be calculated by different methods, the used parameters during this modeling are often based on measurement [1, 15]. However, by knowing the velocity functions, we can define the velocity gradients by Eq. (16), which can be used for calculating the strain values by integrating them along the streamlines.

$$L_{ij} = \frac{\partial v_i}{\partial j}. \quad (16)$$

where, L_{ij} is the ij component of velocity gradient, v_i is the velocity in direction i , and j is the direction used during the derivation. The values of i and j can be x , y and z [51].

There is a modified version of the FLM [51] method, the mFLM method, which is described in [52]. The modified streamline function is given by Eq. (17) [52].

$$\Phi(x, z) = \frac{z}{e} \left[1 + \left(\frac{s}{e} + \left(1 - \frac{s}{e} \right) \left(\frac{d-x}{d} \right)^{2.1} \right)^{-m} \right]^{1/m}, \quad (17)$$

The velocity in direction x can be calculated by Eq. (18) [52].

$$v_x(x, z) = f_1(x) \cdot (1 - z_s)^n + f_2(x) \cdot z_s^n. \quad (18)$$

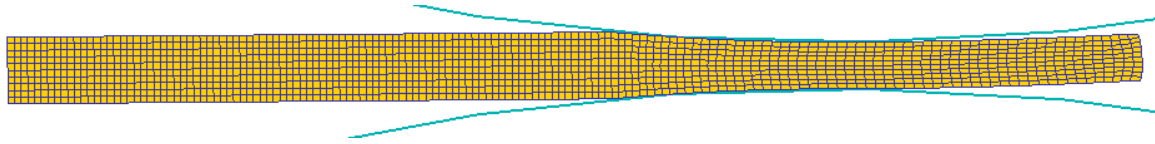


Figure 2. Applied geometry for FEM

The f_1 and f_2 functions can be determined from the boundary condition in form of the Eq. (19)-(21).

$$\frac{1}{n+1}f_1(x) + \frac{1}{n+1}f_2(x) = v_{in} \cdot \left[1 + \left(\frac{s}{e} + \left(1 - \frac{s}{e} \right) \left(\frac{d-x}{d} \right)^{2.1} \right)^{-m} \right]^{1/m}, \tag{19}$$

$$f_2 - f_1 = \alpha \cdot \left\{ e \cdot v_{in} \cdot \left[1 + \left(\frac{s}{e} + \left(1 - \frac{s}{e} \right) \left(\frac{d-x}{d} \right)^{2.1} \right)^{-m} \right]^{1/m} - f_{1,ref} \right\}, \tag{20}$$

$$f_{1,ref} = \left[1 - e^{-a\left(\frac{x}{d}\right)^b} \right] \left(\frac{e}{s}v_{in} - v_{in} \right) + v_{in}. \tag{21}$$

The parameters α and n can be calculated from the geometrical dimensions and technological parameters by using the results of [53].

5. Finite element simulation of rolling

The FEM method is based on separating the bodies into smaller elements and performing further calculations on it. The rolls were modelled as rigid rotating bodies, the sheet as a plastic-elastic material. The 3D model was simplified to a 2D plane strain geometry, by neglecting the TD dimensions. The applied geometry is shown in Fig. 2, the geometrical and technological parameters are the same as for roll tests carried out. The friction coefficient is calculated by the Eq. (5) and (6). The effect of the heat and the strain rate were neglected as it was described in the material model. Simplifications made in frame of the current simulations are the same as for [3, 37]. DEFORM 2D software [46] was employed for simulation of the rolling.

6. Measurement

The deformation flow was investigated in both symmetrically and an asymmetrically rolled sheets. The characteristic parameters for the rolling experiments are shown in Table 1.

The displacement measurement was conducted by using the method described in [3, 69]. Prior to rolling the surface was grinded and polished, and Vickers hardness measurement was performed on the polished TD plane. After cold rolling, the relative displacements were measured between the points. The hardness indents before and after the rolling processes are shown in Fig. 3.

The relative displacement values are determined by the Fiji-ImageJ software package [70, 71], while

Table 1. Characteristic parameters for symmetric and asymmetric rolling tests

Parameter	Symmetric rolling	Asymmetric rolling
Radius of the roll, R [mm]	75	75
Initial thickness of the sheet, h_i , [mm]	1.92	1.92
Sheet thickness following rolling, h_f , [mm]	1.25	1.35
Angular velocity of the top roll, ω_t , [rad/s]	1.1023	1.1023
Angular velocity of the bottom roll, ω_b , [rad/s]	1.1023	0.7480

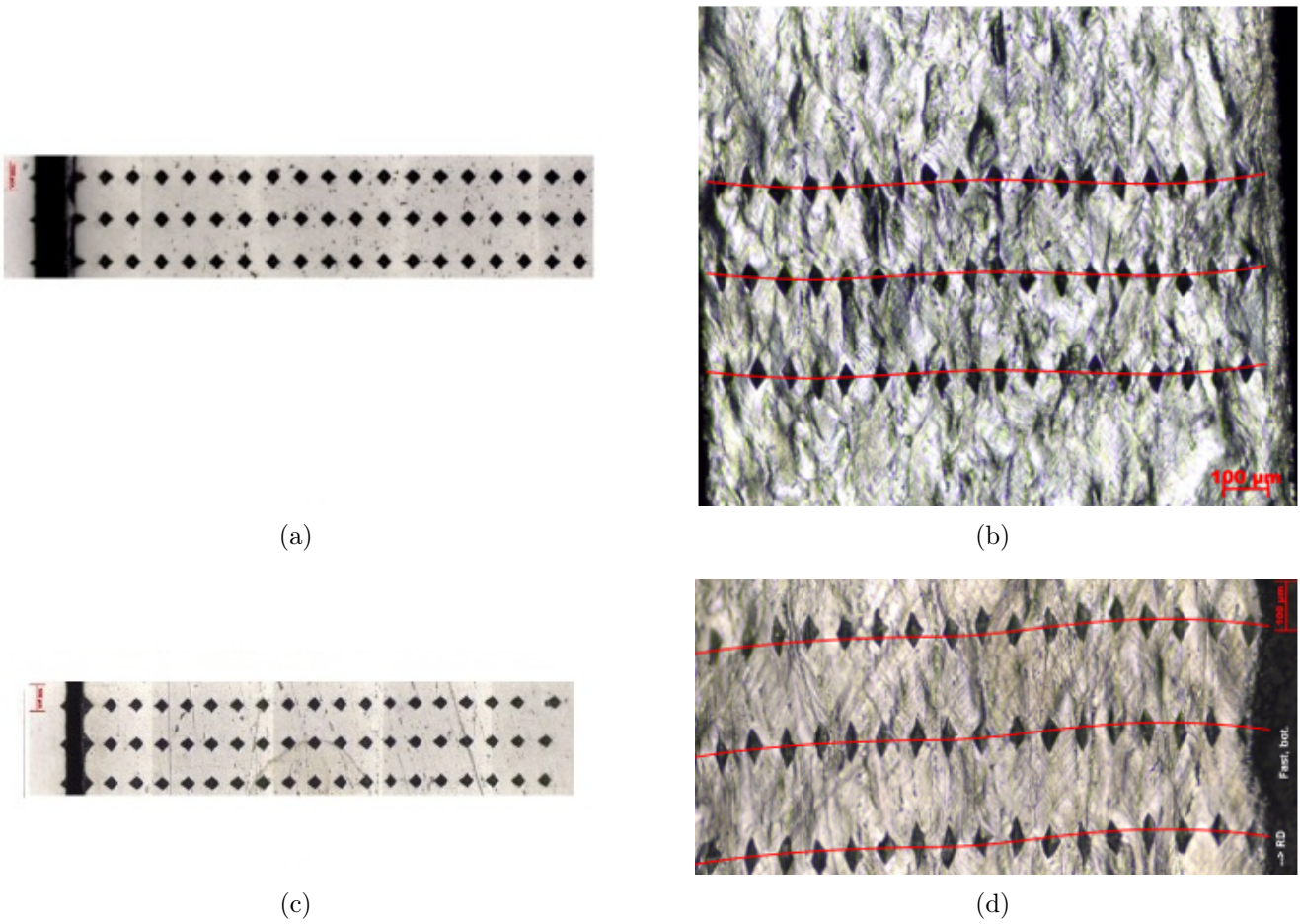


Figure 3. Symmetrically rolled sheet before (a) and after (b) rolling, asymmetrically rolled sheet before (c) and after (d) rolling

the extracted displacements for the symmetric and asymmetric rolling are presented in Fig. 4 and 5, respectively.

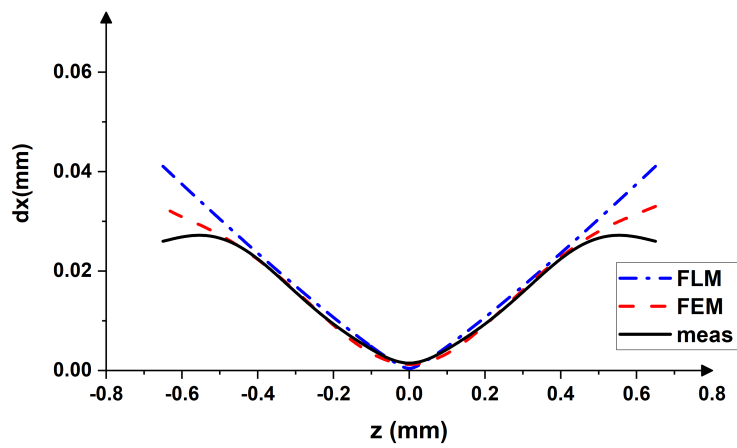


Figure 4. The measured and calculated displacements for the symmetrically rolled sheet

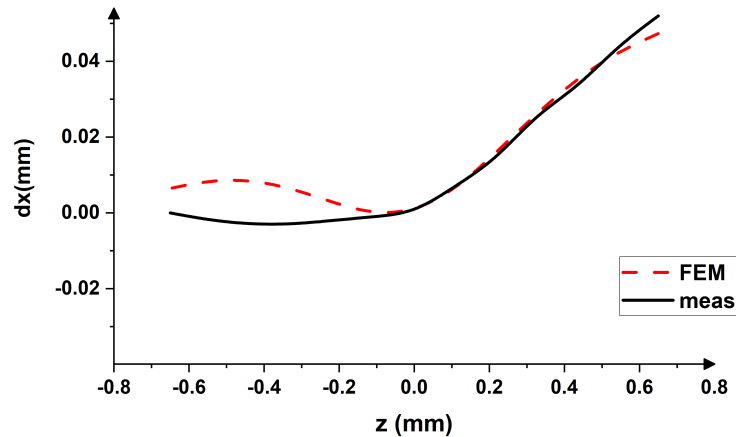


Figure 5. The measured and calculated displacements for the asymmetrically rolled sheet

7. Results

In case of symmetrically rolled sheet, the deviations for the measured three samples are significantly larger, than the measured differences of points' displacements. This deviation is due to the resolution of the applied microscope and the uneven distortion of grains. However, the values calculated by FLM, and FEM methods are comparable. The difference in results is visible in figure 4, where all the measured and calculated results are presented.

Similarly, the results for the asymmetrically rolled sheet are presented in Fig. 5. In this case the FLM method is not applicable, because this approach is valid only for symmetric rolling, the shear cannot be determined by this method. The displacement value near the faster roll is similar for both method; near the slower roll, the difference for the displacement values of different methods are higher, (15% deviation is observed).

Results of the simulations and experimental data, presented in Fig. 4 and 5 suggest that the measured data and the simulated counterparts by FEM and FLM are in a good correlation. It can be concluded here that the calculation methods with the previously described set of parameters are applicable for both symmetric and asymmetric rolling processes.

8. Summary

In this work we have examined different modeling approaches for the simulation of deformation by cold rolling processes. It was shown that the experimentally observed deformation flow can be successfully modelled with the Finite Element Model (FEM) and Flow Line approximation. The advantage of later over FEM is high performance in terms of computational time. The results of FEM and FLM are comparable and accurately reproduce the experimental evidence.

9. Acknowledgement

Project no. TKP2021-NVA-29 has been implemented with the support provided by the Ministry of Innovation and Technology of Hungary from the National Research, Development and Innovation Fund, financed under the TKP2021-NVA funding scheme.

10. References

- [1] J.J Sidor, R.H. Petrov, L. Kestens, *Texture Control in Aluminum Sheets by Conventional and Asymmetric Rolling*, in: Comprehensive Materials Processing, Elsevier, 2014, pp. 447–498. [CrossRef](#)

- [2] S. Geleji, *A fémek képlékeny alakításának elmélete*, Akadémiai Kiadó, Budapest, 1967.
- [3] J.Gy. Bátorfi, J.J. Sidor, *Alumínium lemez aszimmetrikus hengerlése közben fellépő deformációjának vizsgálata*, MéRNöki és Informatikai Megoldások|Engineering and IT Solutions, 2020. I, pp. 5–14, [CrossRef](#)
- [4] J.J. Sidor, Effect of Hot Band on Texture Evolution and Plastic Anisotropy in Aluminium Alloys, *Metals* 11, 2021, 1310, [CrossRef](#)
- [5] J.G. Bátorfi, P. Chakravarty, J. Sidor, *Investigation of the wear of rolls in asymmetric rolling*, MéRNöki és Informatikai Megoldások|Engineering and IT Solutions, 2021. II, pp. 14–20, [CrossRef](#)
- [6] J. Sidor, A. Miroux, R. Petrov, L. Kestens, *Controlling the plastic anisotropy in asymmetrically rolled aluminium sheets*, *Philosophical Magazine* 88, 2008, pp. 3779–3792, [CrossRef](#)
- [7] J. Sidor, R.H. Petrov, L.A.I. Kestens, *Deformation, recrystallization and plastic anisotropy of asymmetrically rolled aluminum sheets*, *Materials Science and Engineering A*. 528, 2010, pp. 413–424, [CrossRef](#)
- [8] O. Engler, V. Randle, *Introduction to texture analysis: macrotexture, microtexture, and orientation mapping*, 2nd edition, CRC Press, Boca Raton, 2010, [CrossRef](#)
- [9] U.F. Kocks, C.N. Tomé, H.-R. Wenk, *Texture and anisotropy: preferred orientations in polycrystals and their effect on materials properties*, Cambridge Univ. Press, Cambridge, 1998.
- [10] P. Chakravarty, G. Pál, J.Gy. Bátorfi, J.J. Sidor, *Estimation of Dislocation Distribution at Mid Thickness for 1050 Al*, *Acta Materialia Transylvanica* 5, 2022, pp. 6–9, [CrossRef](#)
- [11] J. Gubicza, T. Ungár, *Characterization of defect structures in nanocrystalline materials by X-ray line profile analysis*, *Zeitschrift Für Kristallographie - Crystalline Materials* 222, 2007, [CrossRef](#)
- [12] H.J. Bunge, *Texture analysis in materials science: mathematical methods*, Butterworths, London, 1982, [CrossRef](#)
- [13] D. Banabic, H.-J. Bunge, K. Pöhlandt, A.E. Tekkaya, *Formability of Metallic Materials*, Springer Berlin Heidelberg, Berlin, Heidelberg, 2000, [CrossRef](#)
- [14] S.S. Dhinwal, L.S. Toth, *Unlocking Deformation Path in Asymmetric Rolling by Texture Simulation*, *Materials* 13, 2019, 101, [CrossRef](#)
- [15] M. Diehl, *High-resolution crystal plasticity simulations*, 1. Auflage, Apprimus Verlag, Aachen, 2016.
- [16] F. Roters, ed., *Crystal plasticity finite element methods: in materials science and engineering*, Wiley-VCH, Weinheim, 2010, [CrossRef](#)
- [17] F. Roters, M. Diehl, P. Shanthraj, P. Eisenlohr, C. Reuber, S.L. Wong, T. Maiti, A. Ebrahimi, T. Hochrainer, H.-O. Fabritius, S. Nikolov, M. Friák, N. Fujita, N. Grilli, K.G.F. Janssens, N. Jia, P.J.J. Kok, D. Ma, F. Meier, E. Werner, M. Stricker, D. Weygand, D. Raabe, *DAMASK – The Düsseldorf Advanced Material Simulation Kit for modeling multi-physics*

- crystal plasticity, thermal, and damage phenomena from the single crystal up to the component scale*, Computational Materials Science 158, 2019, pp. 420–478, [CrossRef](#)
- [18] F. Roters, P. Eisenlohr, C. Kords, D.D. Tjahjanto, M. Diehl, D. Raabe, *DAMASK: the Düsseldorf Advanced Material Simulation Kit for studying crystal plasticity using an FE based or a spectral numerical solver*, Procedia IUTAM 3, 2012, pp. 3–10, [CrossRef](#)
- [19] F. Roters, P. Eisenlohr, L. Hantcherli, D.D. Tjahjanto, T.R. Bieler, D. Raabe, *Overview of constitutive laws, kinematics, homogenization and multiscale methods in crystal plasticity finite-element modeling: Theory, experiments, applications*, Acta Materialia 58, 2010, pp. 1152–1211, [CrossRef](#)
- [20] J.J. Sidor, *Crystal plasticity and continuum mechanics-based modelling of deformation and recrystallization textures in aluminum alloys*, IOP Conf. Ser.: Mater. Sci. Eng. 375, 2018, 012028, [CrossRef](#)
- [21] J.J. Sidor, *Deformation texture simulation in Al alloys: continuum mechanics and crystal plasticity aspects*, Modelling Simul. Mater. Sci. Eng. 26, 2018, 085011, [CrossRef](#)
- [22] A. Molinari, G.R. Canova, S. Ahzi, *A self consistent approach of the large deformation polycrystal viscoplasticity*, Acta Metallurgica 35, 1987, pp. 2983–2994, [CrossRef](#)
- [23] R.A. Lebensohn, C.N. Tomé, *A self-consistent anisotropic approach for the simulation of plastic deformation and texture development of polycrystals: Application to zirconium alloys*, Acta Metallurgica et Materialia 41, 1993, pp. 2611–2624, [CrossRef](#)
- [24] C.N. Tomé, R.A. Lebensohn, *Manual for Code VISCO-PLASTIC SELF-CONSISTENT (VPSC) - Version 7c*, accessed August 25, 2022, [CrossRef](#)
- [25] Q. Xie, A. Van Bael, J. Sidor, J. Moerman, P. Van Houtte, *A new cluster-type model for the simulation of textures of polycrystalline metals*, Acta Materialia 69, 2014, pp. 175–186, [CrossRef](#)
- [26] P. Eyckens, Q.G. Xie, J.J. Sidor, L. Delannay, A. van Bael, L. Kestens, J. Moerman, H. Vegter, P. van Houtte, *Validation of the Texture-Based ALAMEL and VPSC Models by Measured Anisotropy of Plastic Yielding*, MSF. 702–703, 2011, pp. 233–236, [CrossRef](#)
- [27] C.Q. Ma, L.G. Hou, J.S. Zhang, L.Z. Zhuang, *Strain Analysis during the Symmetric and Asymmetric Rolling of 7075 Al Alloy Sheets*, in: M. Hyland (Ed.), Light Metals 2015, Springer International Publishing, Cham, 2015, pp. 445–449, [CrossRef](#)
- [28] T. Inoue, *Strain Variations on Rolling Condition in Accumulative Roll-Bonding by Finite Element Analysis*, in: D. Moratal (Ed.), Finite Element Analysis, Sciyo, 2010, [CrossRef](#)
- [29] T. Inoue, H. Qiu, R. Ueji, *Through-Thickness Microstructure and Strain Distribution in Steel Sheets Rolled in a Large-Diameter Rolling Process*, Metals 10, 2020, p. 91. [CrossRef](#)
- [30] M. Szűcs, G. Krallics, J.G. Lenard, *The Difficulties of Predicting the Coefficient of Friction in Cold Flat Rolling*, Journal of Tribology 14, 2021, pp. 101703, [CrossRef](#)
- [31] G.-Y. Tzou, *Relationship between frictional coefficient and frictional factor in asymmetrical sheet rolling*, Journal of Materials Processing Technology 86, 1999, pp. 271–277, [CrossRef](#)

- [32] Q.Y. Wang, Y. Zhu, Y. Zhao, *Friction and Forward Slip in High-Speed Cold Rolling Process of Aluminum Alloys*, AMM. 229–231, 2012, pp. 361–364, [CrossRef](#)
- [33] P.P. Gudur, M.A. Salunkhe, U.S. Dixit, *A theoretical study on the application of asymmetric rolling for the estimation of friction*, International Journal of Mechanical Sciences 50, 2008, pp. 315–327, [CrossRef](#)
- [34] L.A. de Carvalho, J. Ebrahim, Z. Lukács, *The Importance of Pressure and Velocity Dependent Friction Coefficient in the Metal Forming Simulation*, GÉP LXXII, 2021, pp. 11–14.
- [35] M. Szűcs, G. Krállics, J. Lenard, *A Comparative Evaluation of Predictive Models of the Flat Rolling Process*, Period. Polytech. Mech. Eng. 2018, [CrossRef](#)
- [36] B. Avitzur, *Friction-aided strip rolling with unlimited reduction*, International Journal of Machine Tool Design and Research 20, 1980, pp. 197–210, [CrossRef](#)
- [37] J.Gy. Bátorfi, G. Pál, P. Chakravarty, J.J. Sidor, *Models for symmetric cold rolling of an aluminum sheet*, EIT, 2022.
- [38] P. Hao, A. He, W. Sun, *Predicting model of thickness distribution and rolling force in angular rolling process based on influence function method*, Mechanics & Industry 19, 2018, p. 302, [CrossRef](#)
- [39] F. Czerwinski, *Thermal Stability of Aluminum Alloys*, Materials 13, 2020, p. 3441, [CrossRef](#)
- [40] B. Gruber, F. Grabner, G. Falkinger, A. Schökel, F. Spieckermann, P.J. Uggowitzer, S. Pogatscher, *Room temperature recovery of cryogenically deformed aluminium alloys*, Materials & Design 193, 2020, 108819, [CrossRef](#)
- [41] P.T. Summers, Y. Chen, C.M. Rippe, B. Allen, A.P. Mouritz, S.W. Case, B.Y. Lattimer, *Overview of aluminum alloy mechanical properties during and after fires*, Fire Sci Rev. 4, 2015, p. 3, [CrossRef](#)
- [42] F. Huang, N.R. Tao, *Effects of Strain Rate and Deformation Temperature on Microstructures and Hardness in Plastically Deformed Pure Aluminum*, Journal of Materials Science & Technology 27, 2011, pp. 1–7, [CrossRef](#)
- [43] Y. Zhao, L. Li, Z. Lu, G. Teng, S. Liu, Z. Hu, A. He, *The effect of annealing temperature on the recrystallization and mechanical properties of severe plastic deformed commercial pure aluminium during ultra-fast annealing*, Mater. Res. Express. 8, 2021, 046515, [CrossRef](#)
- [44] G. Gadamchetty, A. Pandey, M. Gawture, *On Practical Implementation of the Ramberg-Osgood Model for FE Simulation*, SAE Int. J. Mater. Manf. 9, 2016, pp. 200–205, [CrossRef](#)
- [45] W. Ramberg, W.R. Osgood, *Description of stress-strain curves by three parameters*, 1943, accessed November 24, 2021, [CrossRef](#)
- [46] J. Fluhner, *DEFORM(TM) 2D Version 8.1 User's Manual*, [CrossRef](#)
- [47] Y.-M. Hwang, T.-H. Chen, H.-H. Hsu, *Analysis of asymmetrical clad sheet rolling by stream function method*, International Journal of Mechanical Sciences 38, 1996, pp. 443–460, [CrossRef](#)

- [48] S.I. Oh, S. Kobayashi, *An approximate method for a three-dimensional analysis of rolling*, International Journal of Mechanical Sciences 17, 1975, pp. 293–305, [CrossRef](#)
- [49] J.J. Sidor, *Deformation Texture Modelling By Mean-Field And Full-Field Approaches*, AML. 10, 2019, pp. 643–650, [CrossRef](#)
- [50] H.P. Yang, Y.H. Sha, F. Zhang, L. Zuo, *Through-thickness shear strain control in cold rolled silicon steel by the coupling effect of roll gap geometry and friction*, Journal of Materials Processing Technology 210, 2010, pp. 1545–1550, [CrossRef](#)
- [51] B. Beausir, L.S. Tóth, *A New Flow Function to Model Texture Evolution in Symmetric and Asymmetric Rolling*, in: A. Haldar, S. Suwas, D. Bhattacharjee (Eds.), *Microstructure and Texture in Steels*, Springer London, London, 2009, pp. 415–420, [CrossRef](#)
- [52] K. Decroos, J. Sidor, M. Seefeldt, *A New Analytical Approach for the Velocity Field in Rolling Processes and Its Application in Through-Thickness Texture Prediction*, Metall and Mat Trans A. 45, 2014, pp. 948–961, [CrossRef](#)
- [53] J.J. Sidor, *Assessment of Flow-Line Model in Rolling Texture Simulations*, Metals 9, 2019, 1098, [CrossRef](#)
- [54] A. Halloumi, Ch. Desrayaud, B. Bacroix, E. Rauch, F. Montheillet, *A Simple Analytical Model of Asymmetric Rolling*, Archives of Metallurgy and Materials 57, 2012, [CrossRef](#)
- [55] A. Hasani, L.S. Toth, Sh. Mardokh Rouhani, *A New Flow Line Function for Modeling Material Trajectory and Textures in Nonequal-Channel Angular Pressing*, Advances in Materials Science and Engineering, 2019, pp. 1–6, [CrossRef](#)
- [56] A. Hasani, L.S. Tóth, B. Beausir, *Principles of Nonequal Channel Angular Pressing*, Journal of Engineering Materials and Technology 132, 2010, 031001, [CrossRef](#)
- [57] L.S. Tóth, R. Arruffat Massion, L. Germain, S.C. Baik, S. Suwas, *Analysis of texture evolution in equal channel angular extrusion of copper using a new flow field*, Acta Materialia 52, 2004, pp. 1885–1898, [CrossRef](#)
- [58] A. Parvizi, K. Abrinia, *A two dimensional upper bound analysis of the ring rolling process with experimental and FEM verifications*, International Journal of Mechanical Sciences 79, 2014, pp. 176–181, [CrossRef](#)
- [59] B. Avitzur, *An Upper-Bound Approach to Cold-Strip Rolling*, Journal of Engineering for Industry 86, 1964, pp. 31–45, [CrossRef](#)
- [60] Y. Yang, Y. Peng, *Dynamic rolling model based on uniform deformation*, Journal of Manufacturing Processes 58, 2020, pp. 1334–1347, [CrossRef](#)
- [61] C. Yao, A. He, J. Shao, J. Zhao, G. Zhou, H. Li, Y. Qiang, *Finite Difference Modeling of the Interstand Evolutions of Profile and Residual Stress during Hot Strip Rolling*, Metals 10, 2020, 1417, [CrossRef](#)
- [62] A. Ma, F. Roters, D. Raabe, *A dislocation density based constitutive model for crystal plasticity FEM including geometrically necessary dislocations*, Acta Materialia 54, 2006, pp. 2169–2179, [CrossRef](#)

- [63] D. Pustovoytov, A. Pesin, P. Tandon, *Asymmetric (Hot, Warm, Cold, Cryo) Rolling of Light Alloys: A Review*, *Metals* 11, 2021, p. 956, [CrossRef](#)
- [64] D. Pustovoytov, A. Pesin, O. Biryukova, *Finite element analysis of strain gradients in aluminium alloy sheets processed by asymmetric rolling*, *Procedia Manufacturing* 15, 2018, pp. 129–136, [CrossRef](#)
- [65] M. Wronski, K. Wierzbanski, B. Bacroix, P. Lipinski, *Asymmetric rolling textures of aluminium studied with crystalline model implemented into FEM*, *IOP Conference Series: Materials Science and Engineering* 82, 2015, 012012, [CrossRef](#)
- [66] T. Imai, H. Utsunomiya, R. Matsumoto, *Finite Element Analysis of Plastic Instability Phenomenon in Cold Rolling of Clad Sheets*, *Procedia Engineering* 184, 2017, pp. 306–312 [CrossRef](#)
- [67] A. Graça, G. Vincze, *A Short Review on the Finite Element Method for Asymmetric Rolling Processes*, *Metals*. 11, 2021, p. 762, [CrossRef](#)
- [68] H. Wang, S. Ding, T. Taylor, J. Yanagimoto, *Cold Rolling Texture Prediction Using Finite Element Simulation with Zooming Analysis*, *Materials* 14, 2021, p. 6909, [CrossRef](#)
- [69] R. Roumina, C.W. Sinclair, *Deformation Geometry and Through-Thickness Strain Gradients in Asymmetric Rolling*, *Metall and Mat Trans A* 39, 2008, pp. 2495–2503, [CrossRef](#)
- [70] J. Schindelin, I. Arganda-Carreras, E. Frise, V. Kaynig, M. Longair, T. Pietzsch, S. Preibisch, C. Rueden, S. Saalfeld, B. Schmid, J.-Y. Tinevez, D.J. White, V. Hartenstein, K. Eliceiri, P. Tomancak, A. Cardona, *Fiji: an open-source platform for biological-image analysis*, *Nat Methods* 9, 2012, pp. 676–682, [CrossRef](#)
- [71] C.A. Schneider, W.S. Rasband, K.W. Eliceiri, *NIH Image to ImageJ: 25 years of image analysis*, *Nat Methods* 9, 2012, pp. 671–675, [CrossRef](#)